Ionics (2019) 25:3247–3258
https://doi.org/10.1007/s11581-018-2826-6

ORIGINAL PAPER

A comparative and correlation structure-Ac conductivity analysis of doped 1%Eu^{3+} and undoped ceramic of $Li_2BaP_2O_7$

Mariem Beltaif[1] · Marwa Krichen[2] · Makram Megdiche[2] · Mohamed Dammak[1]

Received: 3 September 2018 / Revised: 4 November 2018 / Accepted: 3 December 2018 / Published online: 4 January 2019

Abstract

In this work, $Li_2BaP_2O_7$ doped 1% Eu^{3+} was prepared by a solid-state reaction method and characterized by X-ray diffraction technique, IR, and impedance spectroscopy. Rietveld refinement of the X-ray diffraction pattern suggests the formation of the single-phase desired compound with monoclinic structure at room temperature. Electrical properties were studied using complex impedance spectroscopy in the frequency range of 200 Hz–5 MHz and temperature range of 598–724 K. The temperature dependence of the bulk and grain boundaries' conductivity was found to obey the Arrhenius law with activation energies $E_g = 0.79$ eV and $E_{gb} = 1.85$ eV respectively. Temperature dependence of the power law exponent *s* strongly suggests that tunneling of large polaron is the dominant transport process. The obtained results are compared with the undoped $Li_2BaP_2O_7$ sample and correlated with structural analysis. Doping pyrophosphate compound by Eu^{3+} presents better conductivity and electrical properties.

Keywords Eu^{3+} · Conduction mechanism · AC conductivity · Impedance spectroscopy

Introduction

Rare earth (RE) doped phosphate materials have attracted more and more attention due to their excellent thermal and chemical stability. They have an important role in the development of optical display systems using solid-state lighting such as field emission displays (FEDs), cathode ray tubes, plasma display panels (PDP), optoelectronic devices, biological fluorescence labeling, luminescent paints, and inks for security [1–5]. In order to understand the electrical properties of materials used for solid electrolytes in lithium-ion and to define their physical and chemical parameters, there are two general classes: inorganic ceramics and organic polymers. The pyrophosphates compounds $Li_2MP_2O_7$ (M = Fe, Mn, and Co), which contain P_2O_7 polyanions formed by two PO_4 units sharing one O–O edge, have also been identified as cathode materials for lithium-ion batteries. For this reason, we are interested in this family of compounds, lithium pyrophosphate $Li_2MP_2O_7$ (M = Ba, Zn, Cu …) are members of a large family of compounds of the $A_2BP_2O_7$ type which contain simultaneously an alkali metal ion (A^+) and a divalent cation (B^{2+}). Among these conductive materials, lithium pyrophosphate $Li_2BaP_2O_7$ is mentioned which exhibits interesting magnetic, optical, and electric properties. It is suggested that the $Li_2BaP_2O_7$:Eu^{3+} is a potential host material for laser application [6]. This material is applied in different fields such as energy and electricity, thanks to its high ion or proton mobility [7]. In 2002, Dridi et al. investigated the synthesis and crystal structure of dilithium barium diphosphate $Li_2BaP_2O_7$ [8]. Eu^{3+}/Sm^{3+}- and Ce^{3+}-activated luminescence properties of $Li_2BaP_2O_7$ were reported by Wani et al. [9, 10]. Recently, the electrical properties of $Li_2BaP_2O_7$ were described by Krichen et al. [7].

In this paper, the AC conductivity of the ceramic compound $Li_2BaP_2O_7$:1% Eu^{3+} has been investigated to determine the mechanism for the AC conductivity. The results will be compared with the undoped $Li_2BaP_2O_7$ sample. Interpretation of all results has been correlated with structural analyses.

✉ Mariem Beltaif
mariem.beltaief@yahoo.fr

[1] Laboratoire de Physique Appliquée, Groupe de Physique des matériaux luminescents, Faculté des Sciences de Sfax, Département de Physique, BP 1171, Université de Sfax, 3018 Sfax, Tunisie

[2] Laboratory of Spectroscopic Characterization and Optical Materials, Faculty of Sciences, University of Sfax, B. P. 1171, 3018 Sfax, Tunisia

Experimental procedure

The pyrophosphate $Li_2BaP_2O_7$: 1%Eu^{3+} was obtained by the conventional solid-state reaction. Stoichiometric quantities of lithium carbonate (Li_2CO_3), barium carbonate ($BaCO_3$), erbium oxideEu_2O_3, and ammonium dihydrogen phosphate ($NH_4H_2PO_4$) were of high purity (≥ 99%). The reagents were firstly ground into fine powders using mortar and pestle, intimately mixed, and progressively heated first to 593 K for 8 h to expel gases. The obtained powder was then pressed into cylindrical pellets and heated once at 1023 K for 10 h. A pellet of about 8 mm diameter and about 1.5 mm thickness was used for the optical measurements.

X-ray powder diffraction (XRD) measurements were performed at room temperature by using a Phillips powder diffractometer PW 1710 with CuKα radiation ($\lambda = 1.5405$ Å) at glancing angles between 4° and 94°.

IR spectroscopic analyses were carried out with a FTIR-100 Perkin Elmer spectrophotometer in the wavenumber range of 1300–550 cm^{-1}.

To determine electrical and dielectric properties of the sample, the sintered pellets were sandwiched between two platinum electrodes, heated at 723 K for 1 h, and cooled to room temperature before measurements were performed as a function of both temperature (598–724 K) and frequency (200 Hz–5 MHz) using a TEGAM 3550 ALF impedance analyzer.

Results and discussions

X-ray analysis

The crystal structure of $Li_2BaP_2O_7$ was first reported by Liebertz and Stahr in 1983 [11] who found that it crystallizes in the orthorhombic crystal system with Cmcm space group. More detailed studies have revealed that $Li_2BaP_2O_7$ crystallizes in a monoclinic crystal system with C2/c space group [8].

The X-ray diffraction pattern of Eu^{3+} doped Li2BaP2O7 was recorded at room temperature, along with Rietveld refinement. Experimental, calculated, and shift powder XRD patterns were shown in Fig. 1. The obtained reliability factors are $R_p = 12.5\%$, $R_{wp} = 16.8\%$, $R_{\exp} = 11.9\%$, Bragg R factor = 13.7%, and $\chi^2 = 2.76$. The sample crystallizes in the monoclinic space group C2/c with the following unit cell parameters: $a = 7.084$ (2) Å, $b = 12.160$ (3) Å, $c = 13.85$ (2) Å, and $\beta = 90.69°$. There is a very good agreement between all experiments realized in the same sample, confirming the crystal purity of the synthesized materials. In view of the effective ion radii of cations and disparity valence state, $Li^+ = 0.092$ nm, $Ba^{2+} = 0.142$ nm, it is predicted that $Eu^{3+} = 0.101$ nm may perfectly occupy the different site of Ba^{2+} [9].

Crystal structure of the simple $Li_2Ba_{0.99}Eu_{0.01}P_2O_7$ found that Ba^{2+} is surrounded by 9 oxygen in irregular geometry. Each BaO_5 and EuO_5 polyhedron is surrounded by five PO_4 tetrahedral belonging to three different P_2O_7 groups. The Li^+ ions are located in three different crystallographic sites. Li_1 is irregularly surrounded by five oxygen neighbors (site symmetry C_1), whereas Li_2 and Li_3 exhibit distorted tetrahedral geometry (site symmetry C_2) (Fig. 2). Atomic positions are summarized in Table 1. Interatomic distances and some selected angles are reported in Table 2 for both doped and undoped compound. The main values of P–O–P angles are 123.06° for $Li_2BaP_2O_7$ and 122.93° for $Li_2Ba_{0.99}Eu_{0.01}P_2O_7$.

IR spectroscopy analysis

The infrared bands for undoped $Li_2BaP_2O_7$ and doped $Li_2Ba_{0.99}Eu_{0.01}P_2O_7$ are displayed in Fig. 3. The assignment of the bands is made on the basis that ν_{as} $(PO_3) > \nu_s$ $(PO_3) > \nu_{as}$(P–O–P) > ν_s(P–O–P) > δ (PO_3) > δ(P–O–P).ν_{as} and ν_s refer respectively to asymmetric and symmetric stretching vibrations of P–O bonds in (PO_3) groups or in (P–O–P) bridge; δ refers to deformation modes of (O–P–O) angles.

Since these absorption bands generally overlap, it is not possible to give more precise assignment than that proposed in Table 3. Band assignments for the fundamental modes of $Li_2Ba_{0.99}Eu_{0.01}P_2O_7$ and $Li_2BaP_2O_7$, given in Table 3, confirm the presence of the diphosphate groups in the title compounds [12].

The bands due to the symmetric and antisymmetric stretching frequencies of P–O–P are generally observed in the regions 970–910 cm^{-1} and 770–670 cm^{-1}.

The bands due to δ (PO_3) and δ (P–O–P) deformations are observed in the regions 501–640 $cm^{-1}$and 554–656 cm^{-1} respectively for $Li_2Ba_{0.99}Eu_{0.01}P_2O_7$ and $Li_2BaP_2O_7$.

Electrical impedance analysis

Equivalent circuit study

Equivalent circuit models are described to analyze the electrical response of the sample. Diverse equivalent circuit models have been reported in the literature. Usually, electrical responses, obtained in ceramic materials, are attributed to grain, grain boundary, and electrode effect. Each contribution can be described by a parallel combination of a resistor (R) and a pure capacitor (C) [13] for the ideal response (Debye's model).

These contributions can conventionally be displayed in a complex plane plots (Nyquist diagram) in terms of the same formalism:

Complex impedance:

$$Z^*(\omega) = Z' + jZ'' \quad (1)$$

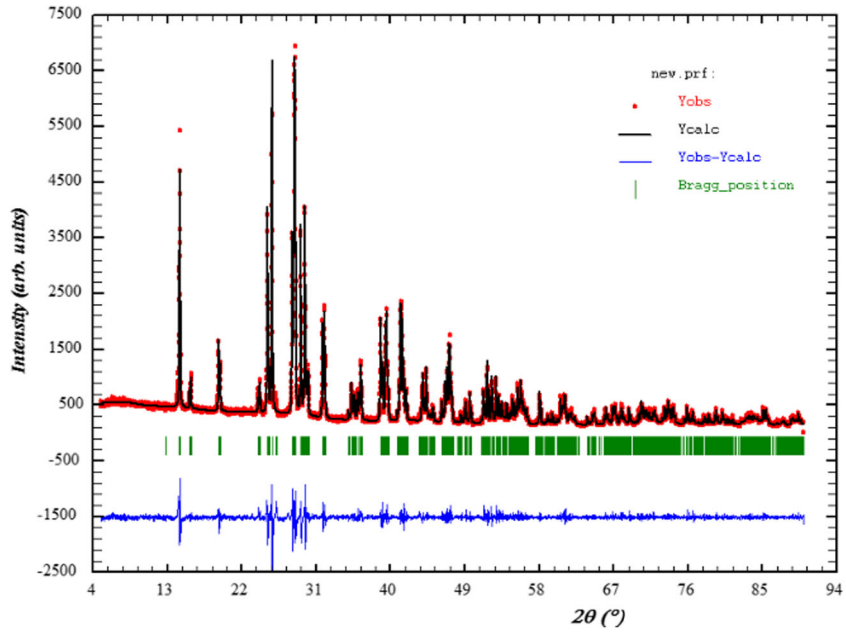

Fig. 1 Powder X-ray diffraction pattern and Rietveld refinement for the sample $Li_2Ba_{0.99}Eu_{0.01}P_2O_7$ (circle signs correspond to experimental data, and the calculated data are represented by the continuous line overlapping them: tick marks represent the positions of allowed reflection, and a difference curve on the same scale is plotted at the bottom of the pattern)

Complex permittivity:

$$\varepsilon^*(\omega) = \varepsilon' - j\varepsilon'' \tag{2}$$

Complex modulus:

$$M^*(\omega) = \frac{1}{\varepsilon^*(\omega)} = M' + jM'' \tag{3}$$

Experimental impedance spectra for the ceramic compound $Li_2Ba_{0,99}Eu_{0,01}P_2O_7$, measured at different temperatures from 598 to 724 K, are shown in Fig. 4a. All diagrams are composed of two successive semicircles which indicate some degree of decentralization. In this case, the centers of semicircles that compose total electric response are centered below of real axis (Z') which confirms the presence of non-Debye type of relaxation in the materials.

To verify the presence of different types of contributions in the studied material, analysis of all relaxation properties can be tested by the modulus representation. Imaginary parts of modulus M'' are calculated by the following equation:

$$M'' = \omega C_0 Z' \tag{4}$$

where ω, C_0, and Z' are angular frequency, vacuum capacitance of cell, and the real parts of the complex impedance respectively. The obtained modulus spectra $M''(\omega)$ versus

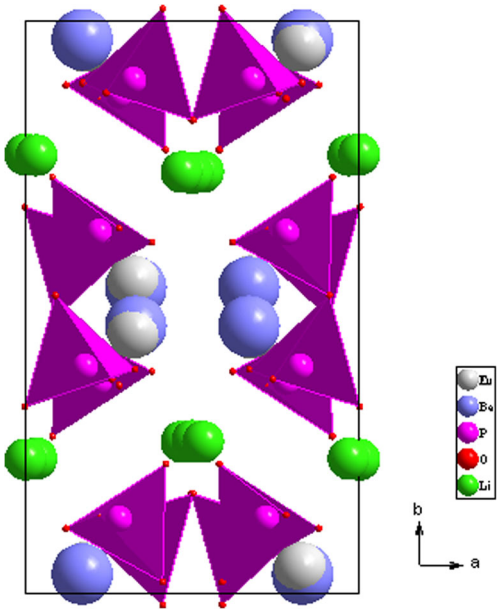

Fig. 2 Crystal structure of $Li_2Ba_{0.99}Eu_{0.01}P_2O_7$

Table 1 Atomic coordinates of $Li_2Ba_{0.99}Eu_{0.01}P_2O_7$

Atom	Wyckoff position	x	y	z
Eu	8f	0.1753(6)	0.0437(3)	0.1008(3)
Ba	8f	0.1697(1)	0.0340(0)	0.1161(5)
P_1	8f	− 0.3222(8)	0.1047(0)	0.1191(4)
P_2	8f	0.2198(3)	0.3697(5)	0.1348(1)
O_1	8f	− 0.1717(0)	0.1094(0)	0.2001(0)
O_2	8f	− 0.2412(0)	0.1263(0)	0.0214(0)
O_3	8f	− 0.5023(0)	0.1742(0)	0.1336(0)
O_4	8f	− 0.4107(0)	− 0.0200(0)	0.1216(0)
O_5	8f	0.0805(4)	0.2739(6)	0.1146(5)
O_6	8f	0.2806(0)	0.3632(1)	0.2394(0)
O_7	8f	0.3788(0)	0.3871(0)	0.0643(0)
Li_1	8f	− 0.4677(0)	0.2646(0)	0.0080(0)
Li_2	4e	0	0.2333(0)	1/4
Li_3	4e	0	− 0.2340(0)	1/4

Table 2 Comparison of angles and interatomic distances with $Li_2BaP_2O_7$ compound

	$Li_2BaP_2O_7$	$Li_2Ba_{0.99}Eu_{0.01}P_2O_7$ (Our study)	
Polyèdre $[P_2O_7]^{4-}$ forme	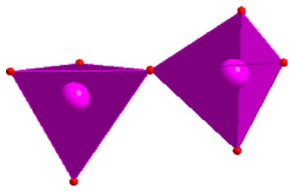 1.501 Å ≤ P-O ≤ 1.640 Å	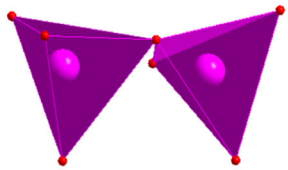 1.499Å ≤P-O≤ 1.641Å	
Angle P-O-P (°)	123.06	122.93	
Polyèdre Ba/Eu	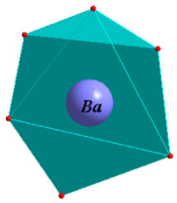 2.679 Å ≤ Ba-O ≤ 2.864 Å	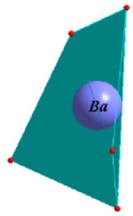 2.695 Å ≤ Ba-O ≤ 2.847 Å	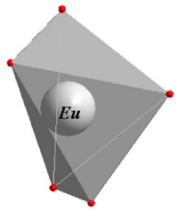 2.462 Å ≤ Eu-O ≤ 2.876 Å
Polyèdre Li_1	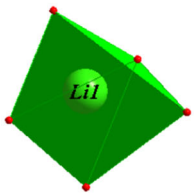 1.952 Å ≤ Li_1-O ≤ 2.330 Å	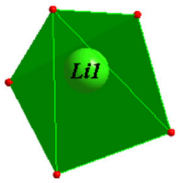 1.927Å ≤Li_1-O≤ 2.330Å	
Polyèdre Li_2	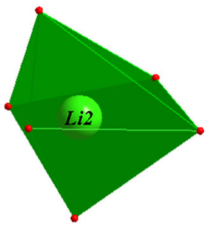 2.048 Å≤ Li_2-O ≤ 2.549 Å	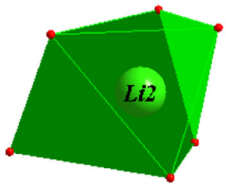 2.026 Å≤ Li_2-O ≤ 2.545 Å	
Polyèdre Li_3	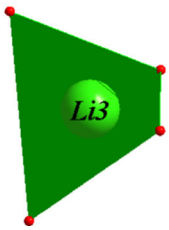 1.957 Å ≤ Li_3-O ≤ 1.966 Å	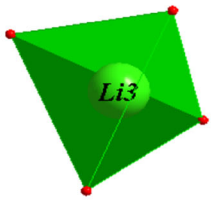 1.957 Å ≤Li_3-O≤ 1.960 Å	

frequency for $Li_2BaP_2O_7$ and $Li_2Ba_{0.99}Eu_{0.01}P_2O_7$ at 724 K is depicted in Fig. 4b. There are two relaxation peaks. Thus, the smaller peak at a lower frequency is associated to grain boundary effects, and the well-defined one at higher frequency is correlated to bulk effects. Thereby, a typical equivalent circuit, consisting of a series of combinations of grains and

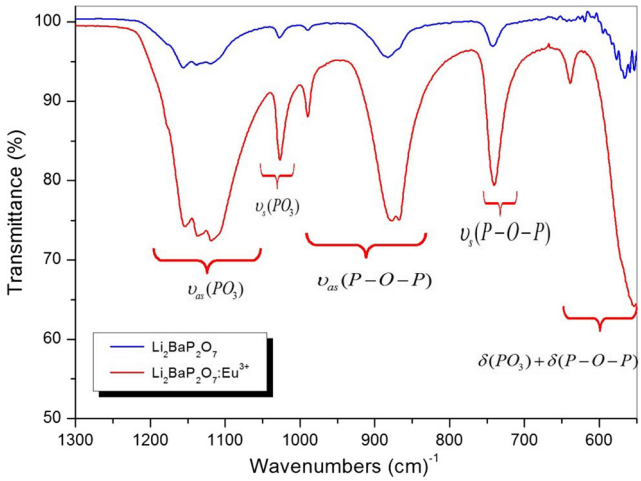

Fig. 3 Infrared analysis spectrum of $Li_2BaP_2O_7$ and $Li_2Ba_{0.99}Eu_{0.01}P_2O_7$

grain boundary elements, was used to fit the measured data. The first consists of a parallel combination of resistance (R_g) and fractal capacitance CPE_1, whereas the second consists of a parallel combination of resistance (R_{gb}), capacitance, and fractal capacitance CPE_2 (inset Fig. 4c).

The expressions of real (Z') and imaginary (Z'') components of impedance related to the equivalent circuit are:

$$Z' = \frac{R_g^2 Q_1 \omega^{\alpha_1} cos\left(\frac{\alpha_1 \pi}{2}\right) + R_g}{\left[1 + R_g Q_1 \omega^{\alpha_1} cos\left(\frac{\alpha_1 \pi}{2}\right)\right]2 + \left[R_g Q_1 \omega^{\alpha_1} sin\left(\frac{\alpha_1 \pi}{2}\right)\right]^2} + \frac{R_{jg}^{-1} + Q_2 \omega^{\alpha_2} \cos\left(\frac{\alpha_2 \pi}{2}\right)}{\left[R_{jg}^{-1} + Q_2 \omega^{\alpha_2} \cos\left(\frac{\alpha_2 \pi}{2}\right)\right]^2 + \left[C\omega + Q_2 \omega^{\alpha_2} \sin\left(\frac{\alpha_2 \pi}{2}\right)\right]^2} \quad (5)$$

Table 3 Assignment of IR bands for $Li_2BaP_2O_7$ and $Li_2Ba_{0.99}Eu_{0.01}P_2O_7$

Compounds	Bands (cm^{-1})	Assignment
$Li_2BaP_2O_7$	1158–1140–1120	$\upsilon_{as}(PO_3)$
	1028	$\upsilon_s(PO_3)$
	990–882	$\upsilon_{as}(P-O-P)$
	741	$\upsilon_s(P-O-P)$
	656–620–608–597–578–566–560–554	$\delta(PO_3)+\delta(P-O-P)$
$Li_2Ba_{0.99}Eu_{0.01}P_2O_7$	1158–1140–1120	$\upsilon_{as}(PO_3)$
	1028	$\upsilon_s(PO_3)$
	990–876	$\upsilon_{as}(P-O-P)$
	738	$\upsilon_s(P-O-P)$
	640–550–518–501	$\delta(PO_3)+\delta(P-O-P)$

$$-Z'' = \frac{R_1^2 Q_1 \omega^{\alpha_1} sin\left(\frac{\alpha_1 \pi}{2}\right)}{\left[1 + R_1 Q_1 \omega^{\alpha_1} cos\left(\frac{\alpha_1 \pi}{2}\right)\right]^2 + \left[R_1 Q_1 \omega^{\alpha_1} sin\left(\frac{\alpha_1 \pi}{2}\right)\right]^2} + \frac{C\omega + Q_2 \omega^{\alpha_2} \sin\left(\frac{\alpha_2 \pi}{2}\right)}{\left[R_2^{-1} + Q_2 \omega^{\alpha_2} \cos\left(\frac{\alpha_2 \pi}{2}\right)\right]^2 + \left[C\omega + Q_2 \omega^{\alpha_2} \sin\left(\frac{\alpha_2 \pi}{2}\right)\right]^2} \quad (6)$$

As shown in Fig. 4a, those diagrams clearly present a good agreement between theoretical (line) and experimental (scatter) data. Consequently, the suggested equivalent circuit describes reasonably well the crystal-electrolyte interface. Fitted values of grain and grain boundary's parameters, for all temperatures, are summarized in Table 4.

The capacitance values of the high- and the low-frequency semicircles are found to be respectively in the range of pF and nF proving that the observed semicircles represent the bulk and grain boundary response of the system respectively [14, 15]. In addition, we note that α_1 values are very close to unity indicating that the interactions between the dipoles are low.

Figure 4c shows the complex impedance plots for $Li_2BaP_2O_7$ and $Li_2Ba_{0,99}Eu_{0,01}P_2O_7$ powder at 609 K and the equivalent circuit model. The modeling of these is carried out with the same equivalent circuit (inset Fig. 4c), whose refinement parameters are summarized in Table 5.

Investigation of DC conductivity

The values of resistance R_g, R_{gb}, and total resistance R_{tot} ($R_{tot} = R_g + R_{gb}$), extracted by equivalent circuit, for each semicircle are used to determine the direct conductivity DC. The DC conductivity (σ_{DC}) has been calculated for each temperature by means of the following relations:

$$\sigma_g = \frac{e}{R_g S} \quad (7)$$

$$\sigma_{gb} = \frac{e}{R_{gb} S} \times \frac{Q_g}{Q_{gb}} \quad (8)$$

$$\sigma_{tot} = \frac{e}{R_{tot} S} = \frac{e}{(R_g + R_{gb}) S} \quad (9)$$

Where e is the thickness ($e = 1$ mm), S is the surface of the sample($S = 0.503$ cm^2), and Q_g and Q_{gb} are respectively the capacitance of grain and grain boundary.

Figure 5 shows that the conductivity obeys the Arrhenius expression of the form:

$$\sigma_{DC} T = \sigma_0 \exp\left(\frac{-E_a}{k_B T}\right) \quad (10)$$

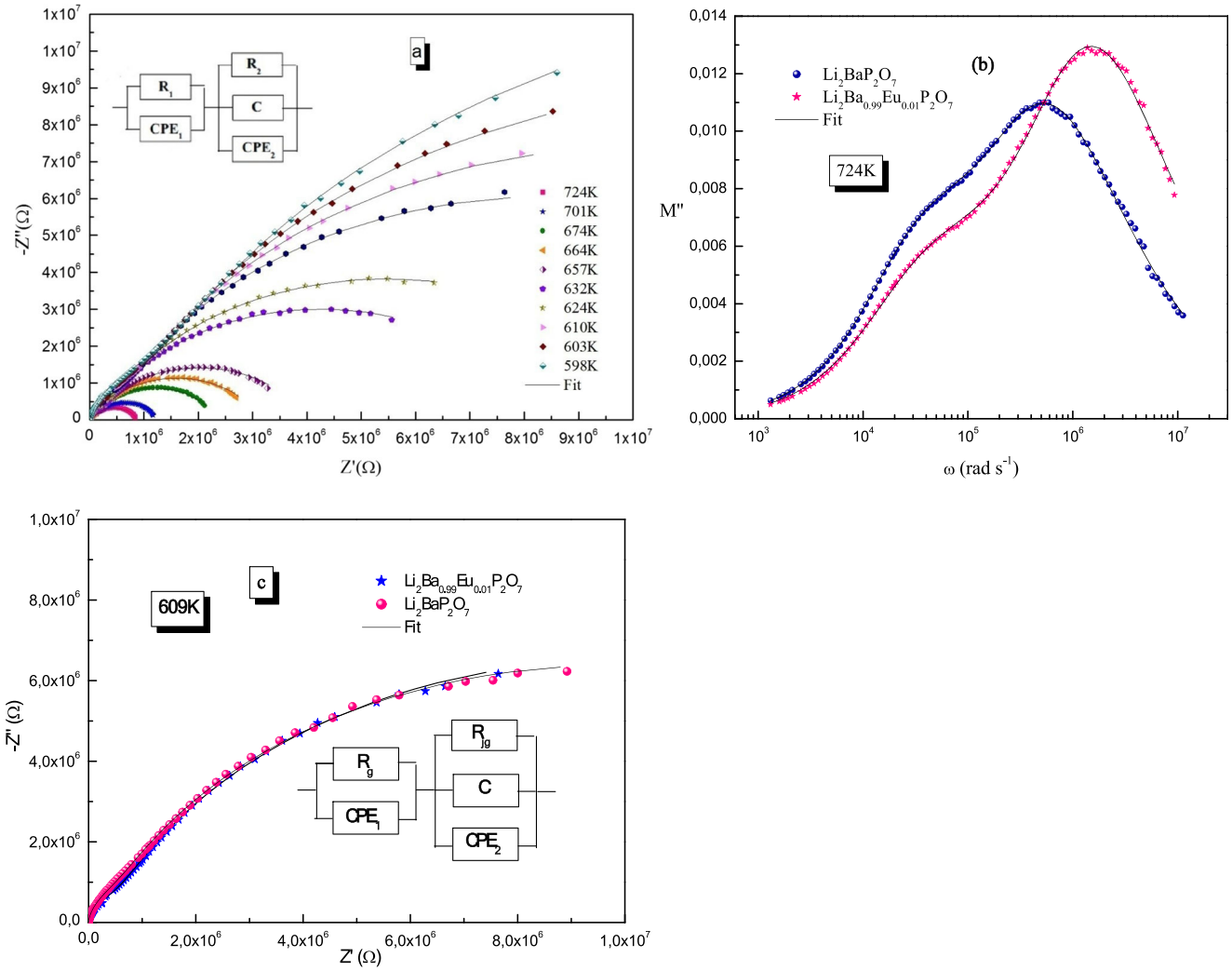

Fig. 4 **a** Complex impedance spectra at various temperatures of $Li_2Ba_{0.99}Eu_{0.01}P_2O_7$ with electrical equivalent circuit. **b** Frequency dependence of the imaginary part M'' at 724 K of $Li_2BaP_2O_7$ and $Li_2Ba_{0.99}Eu_{0.01}P_2O_7$. **c** Complex impedance plots for $Li_2BaP_2O_7$ and $Li_2Ba_{0.99}Eu_{0.01}P_2O_7$ at 609 K and the equivalent circuit model

Where T is absolute temperature, σ_0 is pre-exponential factor, k_B is Boltzmann constant, and E_a is activation energy of the transport process. This plot indicates that electrical conductivity is thermally activated. The value of activation energy, estimated from the Arrhenius plot of σ_g, σ_{gb}, and σ_{tot}, with respect to 1000/T are respectively $E_g = 0.79$ eV, $E_{gb} = 1.85$ eV, and $E_{tot} = 1.23$ eV (Fig. 5).

These later are summarized in Table 6 with some other data such as the grain's conductivity, total conductivity, and the average inter-atomic distances. This table compares the various values obtained by the undoped compound $Li_2BaP_2O_7$ [7]. The conductivity of these compounds can be influenced by factors such as tunnel size, polarizability, and charge carrier mobility. The ease with which an ion can reach a neighboring site is controlled by the activation energy. This latter indicates the barrier of free energy that an ion must overcome to succeed its jump between sites. We note that the studied compound is characterized by the higher activation energies and better conductivity. This result can be explained by the structure of the studied compound. Indeed, the decreasing of the Li–O and Ba–O bond length results to an increase of the attraction force between Li^+, Ba^{2+}, and Eu^{3+} and O^{2-}, and the ions become more attached to the crystal. Structural analyses show that the size of the charge carriers Li^+, inserted in a tunnel, is much wider of the undoped structure. Added to that, the decrease of the number of oxygen forming Barium polyhedron from BaO_6 for the undoped compound to BaO_5/EuO_5 for $Li_2Ba_{0.99}Eu_{0.01}P_2O_7$ may explain the obtained result of conductivity. Consequently, this deformation of structure can prove the highest conductivity of our compound. It produces the increase of potential barrier and requires higher activation energy.

Table 4 Extracted parameters of the equivalent circuit for the $Li_2Ba_{0.99}Eu_{0.01}P_2O_7$ sample

	Grain			Grain boundaries			
T(K)	R_g (10^5 Ω)	Q_1(10^{-11} F)	α_1	R_{gb} (10^7 Ω)	C (10^{-11} F)	Q_2(10^{-10} F)	α_2
598	4.65	3.89	0.962	4.16	1.40	8.08	0.600
603	4.92	4.14	0.951	2.80	1.51	6.31	0.632
610	4.69	4.09	0.947	2.01	1.64	5.42	0.652
618	4.41	4.05	0.949	2.05	1.59	5.71	0.647
624	3.00	4.69	0.938	1.15	1.54	5.03	0.678
632	2.96	5.12	0.927	0.85	1.70	4.32	0.698
652	1.91	4.23	0.941	0.55	1.62	4.51	0.706
657	1.49	5.93	0.923	0.39	1.54	4.21	0.725
664	1.16	7.11	0.918	0.31	1.36	4.17	0.735
674	1.04	6.54	0.913	0.23	1.43	4.05	0.744
683	0.86	7.37	0.911	0.19	1.43	3.89	0.752
692	0.66	7.78	0.913	0.15	1.23	3.85	0.761
701	0.73	9.79	0.892	0.12	1.24	2.80	0.801
712	0.55	13.0	0.878	0.95	1.03	2.91	0.799
724	0.52	15.4	0.868	0.08	1.07	2.62	0.809

AC conductivity analysis

AC measurements are very important for any dielectric material as it gives a lot of information about dynamic properties such as capacitance, conductivity, and loss factor. AC measurements are also helpful in identifying the nature of conduction mechanism.

The complex conductivity can be given as:

$$\sigma^*_{AC} = \sigma' + j\,\sigma'' \tag{11}$$

In the present work, the real and imaginary of complex conductivity were calculated in accordance with the following relation:

$$\sigma' = \frac{e}{s}\left(\frac{Z'}{Z'^2 + Z''^2}\right) \tag{12}$$

$$\sigma'' = \frac{e}{s}\left(\frac{Z''}{Z'^2 + Z''^2}\right) \tag{13}$$

where Z' and Z'' are the real and imaginary part of complex impedance, and e and s are respectively the thickness and the area of the present pellet.

The real part of AC conductivity can be written by following the power law [16]:

$$\sigma_{AC} = \sigma_{DC} + A\omega^S \tag{14}$$

Where σ_{DC} is the direct conductivity in a particular range of temperature, A is a temperature dependent parameter, and s is the temperature-dependent exponent in the range of $0 \le s \le 1$.

This later parameter s presents the degree of interaction between mobile ions with the environments surrounding them, and A determines the strength of polarizability.

Figure 6 presents the frequency dependence of the AC conductivity (σ_{AC}) of $Li_2Ba_{0.99}Eu_{0.01}P_2O_7$ at different temperatures (586–724 K). The AC conductivity increases with the increase of frequency. As illustrated in Fig. 6, these curve increases with increasing of both temperature and frequency.

The classic Jonscher equation (Eq. (14)) does not allow us to explain the behavior of our experimental data. For this, we tried to use the developed Jonscher's equation which gives a better agreement with the experimental values [17]:

$$\sigma_{AC}(\omega) = \frac{\sigma_s + \sigma_\infty \tau 2\omega 2}{1 + \tau 2\omega 2} + A\omega^s \tag{15}$$

Table 5 Comparison of the extracted parameters of the equivalent circuit at 609 K for the $Li_2BaP_2O_7$ and $Li_2Ba_{0.99}Eu_{0.01}P_2O_7$

	R_g (10^5 Ω)	Q_1 (10^{-12} F)	α_1	R_{gb} (10^7 Ω)	C (10^{-11} F)	Q_2 (10^{-10} F)	α_2
$Li_2Ba_{0.99}Eu_{0.01}P_2O_7$	4.69	40.9	0.947	2.01	1.64	5.42	0.652
$Li_2BaP_2O_7$	4.26	43.2	0.969	2.02	1.44	5.55	0.618

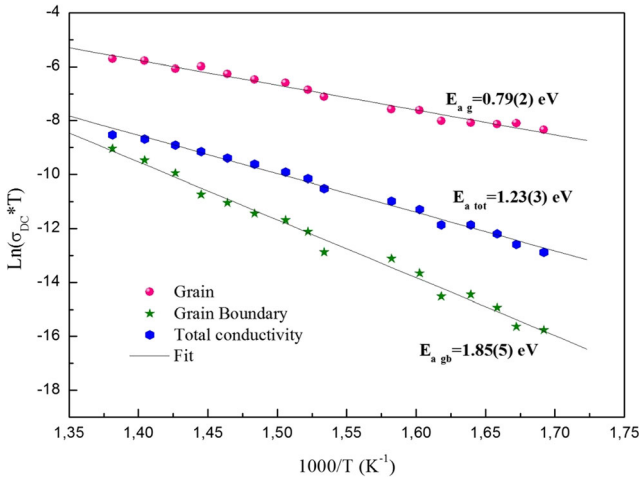

Fig. 5 Variation of the ln (σT) as function of temperature of the $Li_2Ba_{0.99}Eu_{0.01}P_2O_7$ sample

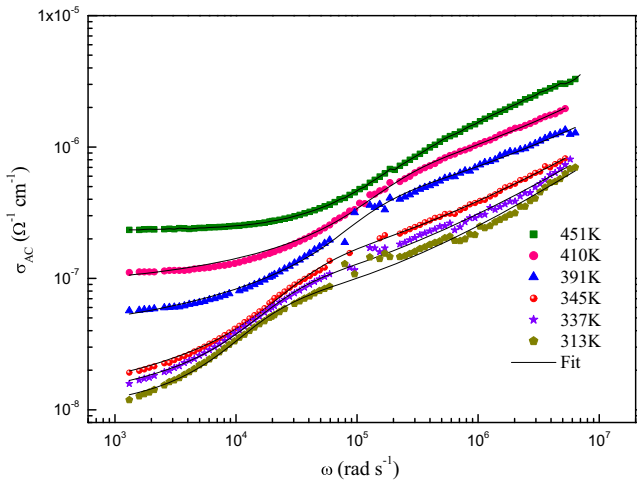

Fig. 6 Frequency dependence of AC conductivity at various temperatures of $Li_2Ba_{0.99}Eu_{0.01}P_2O_7$

In this above equation, σ_s and σ_∞ are respectively an estimate of conductivity at low and high frequencies; ω is angular frequency; and τ represents the characteristic relaxation time.

Frequency dependence of AC conductivity at 683 K of $Li_2BaP_2O_7$ and $Li_2Ba_{0.99}Eu_{0.01}P_2O_7$ is shown in Fig. 7. In high-frequency domain, we note that AC conductivity for $Li_2Ba_{0.99}Eu_{0.01}P_2O_7$ is greater than that obtained for the undoped compound.

As presented in Fig. 6, solid line shows the best modeling of the experimental data by Eq. (15) at different temperatures. This fitting allows us to determine several parameters such as the exponent s. Variation of this parameter s with temperature is illustrated in Fig. 8 for both doped and undoped compound $Li_2Ba_{0.99}Eu_{0.01}P_2O_7$. It seems from this figure that values of s decrease to a minimum value, at about 657 K for $Li_2Ba_{0.99}Eu_{0.01}P_2O_7$, and then increase again with increasing temperature. In addition, thermal variation of this parameter shows a slight evolution in our compound $Li_2Ba_{0.99}Eu_{0.01}P_2O_7$ relative to that of $Li_2BaP_2O_7$. This reflects a weak interaction between the different sites of the free-charge carriers upon insertion of the rare earth ion Eu^{3+} in the matrix $Li_2BaP_2O_7$.

Theory investigation of conduction mechanism

The temperature dependence of s is very useful for determining the type of conduction mechanism in different materials. In the literature, various models have been predicted to explain the temperature dependence of s behavior such as quantum mechanical tunneling (QMT) model, correlated barrier hopping (CBH) model, and the overlapping large-polaron tunneling (OLPT) model [18, 19].

It is seen from Fig. 8 that the values of s, obtained at a different temperature, are less than 0.8 and temperature dependent. Consequently, QMT model is non-applicable to the present electrolyte system. Comparing the results obtained (Fig. 8) with the predicted exponent (s) temperature dependence behavior for CBH and OLPT models, the conduction mechanism for the $Li_2Ba_{0.99}Eu_{0.01}P_2O_7$ compound can be most probably interpreted based on the overlapping large polaron

Table 6 Activations energies and conductivities at 683 K of grain, grains boundaries, total conductivity, and inter-atomic distances in $Li_2BaP_2O_7$ and $Li_2Ba_{0.99}Eu_{0.01}P_2O_7$

Compound		$Li_2BaP_2O_7$	$Li_2Ba_{0.99}Eu_{0.01}P_2O_7$ (our study)
Activation energy (eV)	Grain (E_g)	0.67	0.79
	Grain boundaries (E_{gb})	1.27	1.85
	Total conductivity (E_{tot})	1.08	1.23
Conductivity at 683 K (Ω^{-1} cm^{-1})	Grain (σ_g)	2.17×10^{-6}	2.58×10^{-6}
	Total conductivity (σ_{tot})	1.08×10^{-7}	1.16×10^{-7}
Bond length	< Li–O > (Å)	1.952–2.549	1.927–2.545
	< Ba–O > (Å) < Eu–O > (Å)	2.679–2.864	2.695–2.847 2.462–2.876

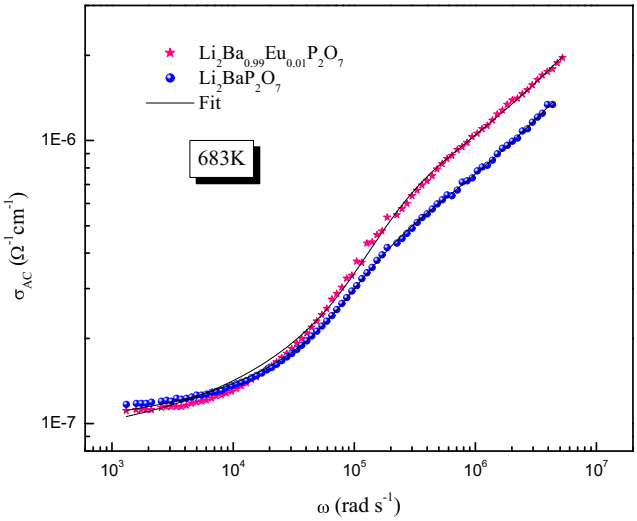

Fig. 7 Frequency dependence of AC conductivity at 683 K of $Li_2BaP_2O_7$ and $Li_2Ba_{0.99}Eu_{0.01}P_2O_7$

tunneling (OLPT) model, where the exponent s decreases with increasing temperature, reaches a minimum at 657 K and, thereafter, increases with temperature.

If overlapping large polaron is formed, the expression for AC conductivity and frequency exponent is given as [20, 21]:

$$\sigma_{AC}(\omega) = \frac{\pi^4}{12} e^2 (k_B T) 2N2 \frac{\omega R_\omega^4}{2\alpha k_B T + \left(W_{H0} r_0 / R_\omega^2\right)} \tag{16}$$

The exponent s is given by:

$$s = 1 - \frac{8\alpha R_\omega + \frac{6 W_{HO} r_0}{R_\omega k_B T}}{\left[2\alpha R_\omega + \frac{W_{HO} r_0}{R_\omega k_B T}\right]^2} \tag{17}$$

where R_ω is the hopping length at angular frequency ω (is the tunneling distance), r_p is the polaron radius, ε_p is the effective

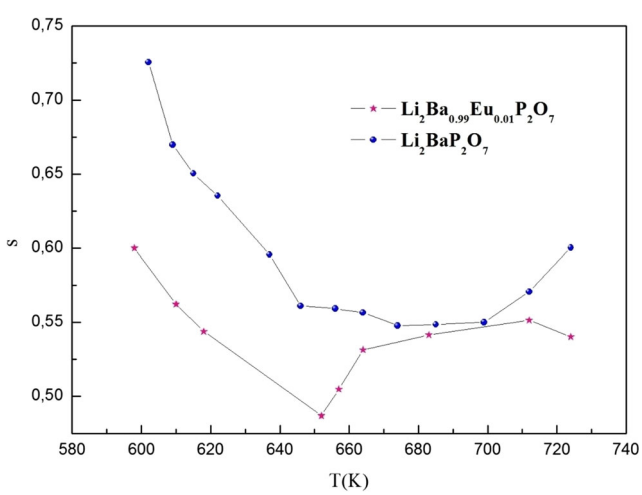

Fig. 8 Temperature dependence of the exponent s for both $Li_2BaP_2O_7$ and $Li_2Ba_{0.99}Eu_{0.01}P_2O_7$

dielectric constant of the material, α is inverse localization length, and N is the density of defect states.

Dielectric study

Studies of the electrical conductivity's frequency-dependent of materials are important to explain the mechanisms of conduction in these materials. Furthermore, dielectric relaxation studies are important too. In the first place, it reveals significant information about the chemical as well as physical behavior. This, in turn, may be useful in the determination of the structure and defects in solids [22, 23]. Real ε' and imaginary parts ε'' of dielectric are calculated using the formula:

$$\varepsilon^* = \frac{1}{j\omega C Z^*} = \varepsilon' + j\varepsilon'' \tag{18}$$

where Z^* is the complex impedance, $C = \frac{\varepsilon_0 A}{d}$, A is the effective area of the electrodes, d is the thickness of the pellet, ε_0 is the vacuum permittivity, and ω is angular frequency.

In this case, the dielectric relaxation is described by a non-Debye model which gives the frequency-dependent complex permittivity in the form [22]:

$$\varepsilon^*(\omega) = \varepsilon_\infty + \frac{\varepsilon_s - \varepsilon_\infty}{1 + \left(j\frac{\omega}{\omega_1}\right)^{1-\alpha}} + \frac{\sigma_{DC}}{j\varepsilon_0 \omega} \tag{19}$$

Where σ_{DC} represents the specific conductivity, ε_s is the static permittivity, ε_0 is the permittivity of free space, ε_∞ is the high-frequency value of ε', α is the distribution of relaxation time ($0 < \alpha < 1$), and ω_1 is the frequency of relaxation of the Debye process.

Real and imaginary parts of ε^* are given by the following expression:

$$\varepsilon'(\omega) = \frac{(\varepsilon_s - \varepsilon_\infty)\left[1 + \left(\frac{\omega}{\omega_1}\right)^{1-\alpha} \cos\frac{(1-\alpha)\pi}{2}\right]}{1 + 2\left(\frac{\omega}{\omega_1}\right)^{1-\alpha} \cos\frac{(1-\alpha)\pi}{2} + \left(\frac{\omega}{\omega_1}\right)^{2(1-\alpha)}} \tag{20}$$

$$\varepsilon''(\omega) = \frac{(\varepsilon_s - \varepsilon_\infty)\left(\frac{\omega}{\omega_1}\right)^{1-\alpha} \sin\left(\frac{(1-\alpha)\pi}{2}\right)}{1 + 2\left(\frac{\omega}{\omega_1}\right)^{1-\alpha} \cos\frac{(1-\alpha)\pi}{2} + \left(\frac{\omega}{\omega_1}\right)^{2(1-\alpha)}} + \frac{\sigma_{DC}}{\varepsilon_0 \omega} \tag{21}$$

As far as illustrated in Fig. 9a and Fig. 9b, it shows the frequency dependence of real and imaginary part of the dielectric constant at 683 K for both studied compound, $Li_2BaP_2O_7$ and $Li_2Ba_{0.99}Eu_{0.01}P_2O_7$, respectively in Fig. 9a and Fig. 9b. The best fit, using Eq. (21), generates a suitable

fitting of the curves resulting from experimental data (solid line in Fig. 9b).

From these curves, we note that the imaginary part of permittivity ε'' decreases rapidly at low frequency without any relaxation; this confirms that the dielectric behavior of this material does not obey the law of Debye. It is important to mention that there are no substantial relaxation peaks in the frequency range employed in this study. Furthermore, the dielectric loss rises sharply at low frequency indicating that electrode polarization and space charge effects have occurred confirming non-Debye dependence [24].

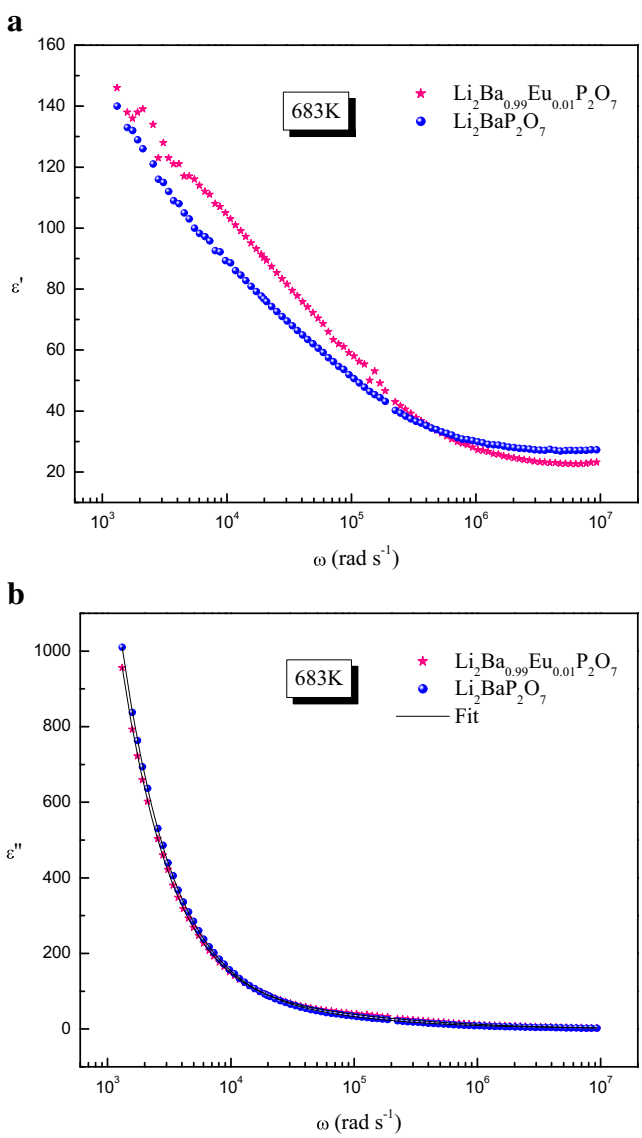

Fig. 9 **a** Frequency dependence of the real part of the dielectric constant at 683 K for $Li_2BaP_2O_7$ and $Li_2Ba_{0.99}Eu_{0.01}P_2O_7$. **b** Frequency dependence of the imaginary part of the dielectric constant at 683 K for $Li_2BaP_2O_7$ and $Li_2Ba_{0.99}Eu_{0.01}P_2O_7$

Modulus study

An alternative approach to investigate the electrical response of materials that present some degree of ionic conductivity is to use the complex electric modulus:

$$M^*(\omega) = \frac{1}{\varepsilon^*(\omega)} = M' + jM'' \tag{22}$$

This formalism is particularly suitable to detect phenomena as electrode polarization [25] and bulk phenomenon property as average conductivity relaxation times τ [26–28].

The variation of the frequency dependence of M'' (ω) for $Li_2Ba_{0.99}Eu_{0.01}P_2O_7$ is shown in Fig. 10. Two peaks are observed in these curves for all temperature: one at low frequency which corresponds the grain boundary relaxation, while the second one, detected at high frequency, is correlated to grain interior.

As already established for the compound $Li_2BaP_2O_7$, the imaginary part of the electric modulus of our compound has been fitted for different temperatures with an approximate frequency representation of the Kohlrausch–Williams–Watts (KWW) function, proposed by Bergman [7]:

$$M'' = \frac{M''_{1\,\max}}{\left((1-\beta_1) + \left(\frac{\beta_1}{1+\beta_1}\right)\right)\left[\left(\frac{\omega_{1\,\max}}{\omega}\right) + \left(\frac{\omega}{\omega_{1\,\max}}\right)^{\beta_1}\right]} + \frac{M''_{2\,\max}}{\left((1-\beta_2) + \left(\frac{\beta_2}{1+\beta_2}\right)\right)\left[\left(\frac{\omega_{2\,\max}}{\omega}\right) + \left(\frac{\omega}{\omega_{2\max}}\right)^{\beta_2}\right]} \tag{23}$$

where $M_{\max}$ and $\omega_{\max}$ are respectively the modulus and the frequency maximum. The value of β is positioned in the 0–1 range, which reflects the importance of coupling between mobile ions in the conduction process.

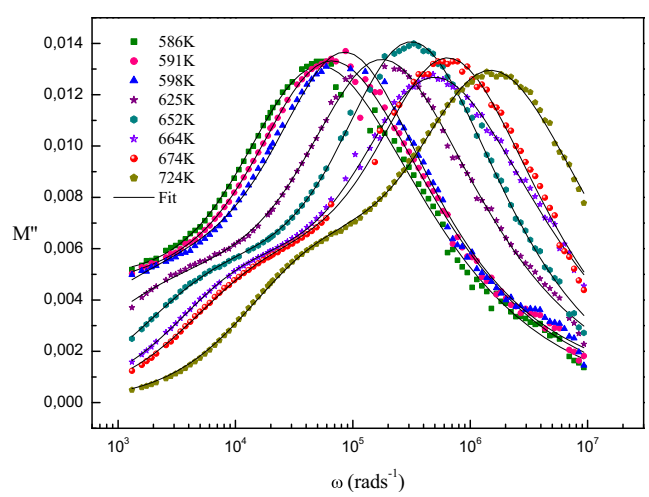

Fig. 10 Frequency dependence of the imaginary part of electric modulus at several temperatures

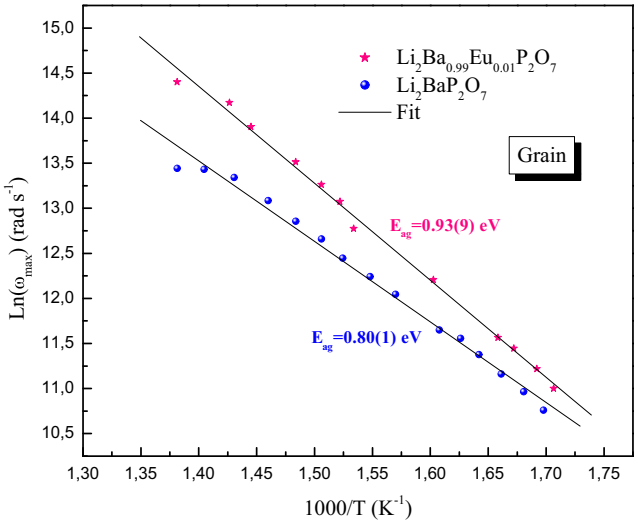

Fig. 11 Temperature dependence of the grain relaxation frequency for $Li_2BaP_2O_7$ and $Li_2Ba_{0.99}Eu_{0.01}P_2O_7$

The relaxation frequency ω_{max}, extracted from the fit of the modulus for both the doped and undoped compound, is presented as function of temperature for grain and grain boundary respectively in Figs. 11 and 12. These curves follow the Arrhenius relation:

$$\omega_{max} = \omega_0 \exp\left(\frac{-E_a}{k_B T}\right) \quad (24)$$

Where ω_0 is the frequency at infinite temperature and E_a is the activation energy. The activation energy determined of grain and grain boundary, for both studied compound $Li_2Ba_{0.99}Eu_{0.01}P_2O_7$ and $Li_2BaP_2O_7$, is summarized in Table 7.

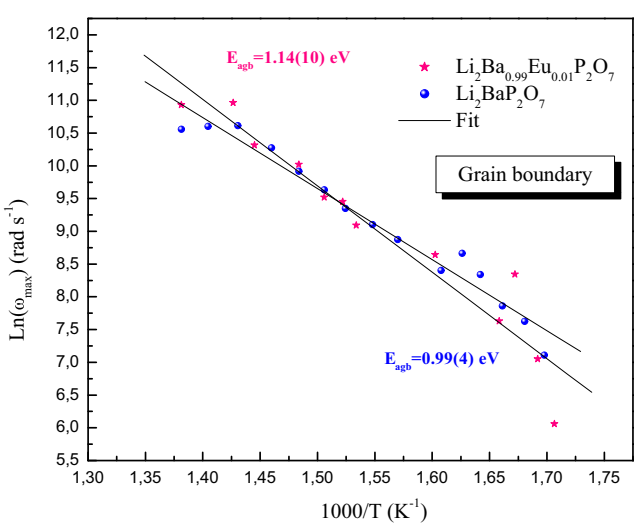

Fig. 12 Temperature dependence of the grain boundary relaxation frequency for $Li_2BaP_2O_7$ and $Li_2Ba_{0.99}Eu_{0.01}P_2O_7$

Table 7 Activation energy of $Li_2BaP_2O_7$ and $Li_2Ba_{0.99}Eu_{0.01}P_2O_7$ from modulus

	$Li_2BaP_2O_7$	$Li_2Ba_{0.99}Eu_{0.01}P_2O_7$ (our study)
Grain E_{ag} (eV)	0.80(1)	0.93(9)
Grain boundary E_{agb} (eV)	0.99(4)	1.14(10)

The obtained values are different from that obtained by conductivity σ_{DC} which proves that conduction and relaxation do not follow the same mechanism. Added to that, frequency variation of M'' at the temperature $T = 724$ K, as shown in Fig. 4b, we notice a faster relaxation of dipole moments in the doped compound $Li_2Ba_{0.99}Eu_{0.01}P_2O_7$; indeed, the maximum angular frequency of relaxation of the modulus M'' of $Li_2Ba_{0.99}Eu_{0.01}P_2O_7$ is higher than that of $Li_2BaP_2O_7$ ($\omega\tau = 1$).

Conclusion

In this work, we have synthesized the $Li_2BaP_2O_7$ doped with 1% Eu^{3+} compound by solid-state method. Rietveld refinement indicates that the sample is single-phase. The impedance plots show two semicircles, which confirm the presence of two relaxation processes associated with the grain and grain boundaries. The OLPT model was found to explain successfully the mechanism of charge transport in $Li_2BaP_2O_7$:Eu^{3+}. A comparative study of structural, vibrational, electric, and dielectric aspects was carried out with the undoped compound $Li_2BaP_2O_7$. The AC conductivity study shows that the doped compound has a better electrical property. This result can be interpreted on the basis of structural analyses which shows that the charge carriers responsible of conduction for Li^+ inserted in a tunnel whose size is much wider of undoped structure, the interaction of Li^+ ion with oxygen atoms decreases ($s_{doped} < s_{undoped}$: the s represents the degree of interaction between mobile ions with the environments surrounding them) which increases their polarizability factor. Consequently, doping of 1% Eu^{3+} in the Ba^{2+} sites improves the electrical conductivity and dielectric properties.

References

1. Zhong J, Liang H, Han B, Su Q, Tao Y (2008) $NaGd(PO_3)_4$: Tb^{3+} A new promising green phosphor for PDPs application. Chem Phys Lett 453:192–196
2. Zhu J, Cheng WD, Wu DS, Zhang H, Gong YJ, Tong HN, Zhao D (2008) Crystal and band structures, and optical characterizations of

sodium rare earth phosphates $NaLnP_2O_7$ and NaLn $(PO_3)_4$(Ln = Ce, Eu). Alloys Compd 454:419–426
3. Chipaux R, Cribier M, Dujardin C, Garnier N, Guerassimova N, Mallet J, Meyer JP, Pedrini C, Petrosyan AG (2002) Ytterbium-based scintillators, a new class of inorganic scintillators for solar neutrino spectroscopy. Nucl Instrum Methods Phys Res A 486: 228–233
4. Ferhi M, Horchani-Naifer K, Ferid M (2008) Hydrothermal synthesis and photoluminescence of the monophosphate $LaPO_4$:Eu(5%). Lumin 128:1777–1782
5. Ferhi M, Horchani-Naifer K, Ferid M (2009) Combustion synthesis and luminescence properties of $LaPO_4$: Eu (5%). Rare Earths 27: 182–186
6. Beltaif M, Dammak M, Megdiche M, Guidara K (2016) Synthesis, optical spectroscopy and Judd–Ofelt analysis of Eu^{3+} doped $Li_2BaP_2O_7$ phosphors. Lumin 177:373–379
7. Krichen M, Megdiche M, Guidara K, Gargouri M (2015) AC conductivity and mechanism of conduction study of lithium barium pyrophosphate $Li_2BaP_2O_7$ using impedance spectroscopy. Ionics 21:935–948
8. Dridi N, Arbib E, Boukhari A, Holt EM (2002) Dilithium barium diphosphate. Acta Crystallogr C 58:74–75
9. Wani JA, Dhoble NS, Kokode NS, DevaPrasadRaju B, Dhoble SJ (2014) Synthesis and luminescence property of $Li_2BaP_2O_7$: Ln^{3+}(Ln= Eu, Sm) phosphors. Lumin 147:223–228
10. Wani JA, Dhoble NS, Dhoble SJ (2012) Photoluminescence characterization of $Li_2BaP_2O_7$:Ce^{3+} phosphor. Int J Knowl Eng 3:130–131
11. Liebertz J, Stahr S (1983) $Li_2BaP_2O_7$: Einkristallzüchtung, Metrik und Raumgruppe. Z Krist 162:313–314
12. Ayed B (2012) Crystal structure and ionic conductivity of $AgCr_2(PO_4)(P_2O_7)$. C R Chimie 15:603–608
13. Mac Donald JR (1987) Impedance spectroscopy: emphasizing solid materials and systems. John Wiley and Sons, New York
14. Mahamoud H, Louati B, Hlel F, Guidara K (2011) Impedance and modulus analysis of the $(Na_{0.6}Ag_{0.4})_2PbP_2O_7$ compound. Alloys Compd 509:6083–6089
15. Megdiche M, Perrin-pellegrino C, Gargouri M (2014) Conduction mechanism study by overlapping large-polaron tunnelling model in $SrNiP_2O_7$ ceramic compound. Alloys Compd 584:209–215
16. Jonscher AK (1977) The universal dielectric response. Nature 267: 673–679
17. Dussouze M (2005) Second harmonic generation in glasses borophosphate sodium and niobium thermal polarization. Thesis, University Bordeaux I (France)
18. Elliott SR (1977) A theory of ac conduction in chalcogenide glasses. Philos Mag B 36:1291–1304
19. Pike GE (1972) AC conductivity of scandium oxide and a new hopping model for conductivity. Phys Rev B: Condens Matter 6: 1572–1580
20. Ghosh A, Bhattacharya S, Ghosh A (2008) Frequency dependent conductivity of cadmium vanadate glassy semiconductor. J Phys Condens Matter 20:035203–035208
21. Long AR (1982) Frequency-dependent loss in amorphous semiconductors. Adv Phys 31:553–637
22. Moynihan CT, Boesch LB, Laberge NL (1973) The Debye-Falkenhagen theory of electrical relaxation in glass. Phys Chem Glasses 14:122
23. Macedo PB, Moynihan CT, Bose R (1972) The role of ionic diffusion in polarization in vitreous ionic conductors. Phys Chem Glasses 13:171
24. Qian X, Gu N, Cheng Z, Yang X, Dong S (2001) Impedance study of (PEO)10$LiClO_4$–Al_2O_3 composite polymer electrolyte with blocking electrodes. Electrochim Acta 46:1829–1836
25. Almond DP, West AR (1983) Impedance and modulus spectroscopy of "real" dispersive conductors. Solid State Ionics 11:57–64
26. Gerhardt R (1994) Impedance and dielectric spectroscopy revisited: distinguishing localized relaxation from long-range conductivity. J Phys Chem Solids 55:1491–1506
27. Reau JM, Jun XY, Senegas J, Le Deit C, Poulain M (1997) Influence of network modifiers on conductivity and relaxation parameters in some series of fluoride glasses containing LiF. Solid State Ionics 95:191–199
28. Bobe JM, Reau JM, Senegas J, Poulain M (1995) F^- ion conductivity and diffusion properties in ZrF^{4-}based fluoride glasses with various NaF concentrations (0⩽ xNaF⩽ 0.45. Solid State Ionics 82: 39–52